Hindawi Publishing Corporation
Journal of Nanomaterials
Volume 2015, Article ID 763617, 8 pages
http://dx.doi.org/10.1155/2015/763617

Research Article

Enhancement of Visible Upconversion Emission in Y_2O_3:Er^{3+}-Yb^{3+} by Addition of Thiourea and LiOH in the Phosphor Synthesis

Eder Resendiz-L,[1] Luis Armando Diaz-Torres,[2] Luis Octavio Meza Espinoza,[3] Claramaria Rodríguez-González,[1] and Pedro Salas[1]

[1]*Centro de Física Aplicada y Tecnología Avanzada, Universidad Nacional Autónoma de México, Apartado Postal 1-1010, Santiago de Querétaro, QRO, Mexico*
[2]*Grupo de Espectroscopia de Materiales Avanzados y Nanoestructurados (GEMANA), Centro de Investigaciones en Óptica, Apartado Postal 1-948, León, GTO, Mexico*
[3]*Instituto de Física, Benemérita Universidad Autónoma de Puebla, Apartado Postal J-48, Centro Histórico, 72570 Puebla, Mexico*

Correspondence should be addressed to Luis Armando Diaz-Torres; ditlacio@cio.mx

Received 30 August 2015; Accepted 8 November 2015

Academic Editor: Bin Dong

Spherical like Y_2O_3 nanostructures doped with Er^{3+} and Yb^{3+} ions have been synthesized by a facile hydrothermal method. The samples were prepared by using different precipitant agents in the synthesis process. The phosphors were characterized by X-ray diffraction (XRD), scanning electron microscopy (SEM), and photoluminescence spectroscopy. Effects of the precipitant agents on structural, morphological, and photoluminescence properties of Y_2O_3:Er^{3+}-Yb^{3+} are studied and discussed. XRD analysis indicates that all samples, prepared with different precipitant agents, present the same cubic phase. Electron microscopy measurements show regular spherical shapes with size diameter depending on precipitant agent. Photoluminescence reveals that the samples have strong green (563 nm) and red (660 nm) emissions corresponding to $^4S_{3/2} \rightarrow {}^4I_{15/2}$ and $^4F_{9/2} \rightarrow {}^4I_{15/2}$ transitions of Er^{3+} ions, respectively. The nanophosphors prepared with both Thiourea and Lithium Hydroxide exhibit the stronger visible upconversion luminescence under 980 nm diode laser excitation.

1. Introduction

In recent years the interest in nanophosphor materials doped with rare earth ions has been growing due to their wide practical applications such as high performance phosphors [1], biomedicine diagnosis [2], solid state lasers [3], sensors [4, 5], and biotechnological applications [6]. These materials have important characteristics due to the upconversion processes which convert near-infrared photons into visible photons via the multiphonon processes [7]. It is well known that yttrium oxide (Y_2O_3) is a commonly used luminescent host material which is known as one of the most promising fluorescent materials when doped with rare earth ions like Yb^{3+} [8], Er^{3+} [5, 9], a combination of Yb^{3+} and Er^{3+} ions [5, 10, 11], and a combination of other ones [11–20]. Due to its low phonon energy, this host lattice promotes the conversion of near-infrared radiation (NIR) into shorter wavelengths emissions, such as visible and UV, when doped with rare earth ions.

Yttrium oxide (Y_2O_3) has excellent physical and chemical properties such as a large transparency range of about 2.8–8 μm, high melting point (2450°C), large energy band gap (5.8 eV), and relatively low phonon energy (about 500 cm^{-1}) [9, 10]. Y_2O_3 doped with sensitizer and activator ions such as Yb^{3+} and Er^{3+}, respectively, has been established as one model for upconversion systems to generate visible emission under IR laser excitation. The sensitizer ion (Yb^{3+}) is excited with near-infrared radiation source and transfers its energy to the activator ion (Er^{3+}) that in turn emits a visible photon.

Several studies have examined the luminescence properties of yttrium oxide nanocrystals doped with rare earth ions.

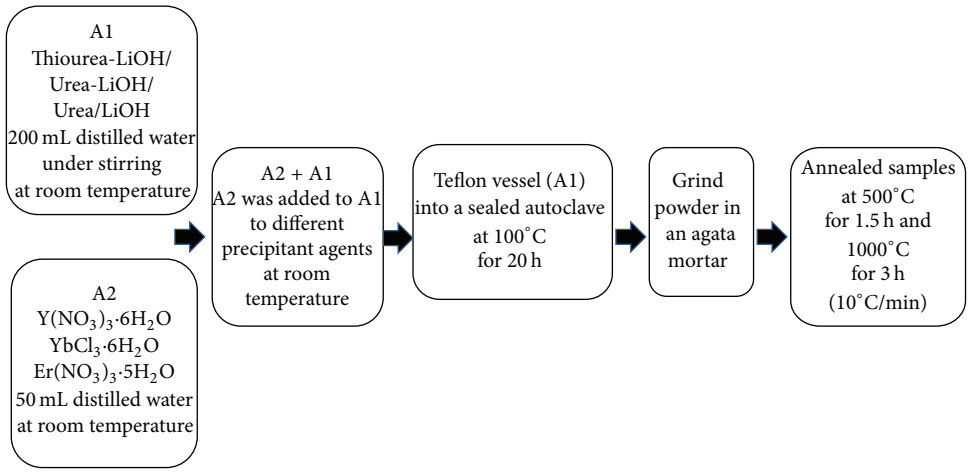

Figure 1: Schematic diagram of the steps for the synthesis method.

Y_2O_3:Eu^{3+} phosphor powders have been prepared by the sol-combustion synthesis method using a sulfur-containing organic fuel in an ethanol-aqueous solution [20, 21]. Upconversion luminescence in Y_2O_3:Er^{3+}-Yb^{3+} nanocrystals as a function by tridoping with different contents of Li ion was investigated [18, 21–24]. However, the effects on photoluminescence properties of Li and S ions have not yet been investigated. In this work, Er^{3+}:Yb^{3+} codoped Y_2O_3 nanophosphors via hydrothermal synthesis had been obtained by adding Lithium Hydroxide and Thiourea in the synthesis process, as sources of Li and S ions, respectively. The obtained nanostructures present spherical shapes, narrow size distribution, and the same crystalline phase, and the color emission of the nanophosphors presents high upconversion luminescence emission.

2. Experimental Details

2.1. Preparation of Y_2O_3:Er^{3+}-Yb^{3+} Nanocrystals. All chemicals were of analytical grade from Aldrich Inc. and used as received. Deionized water was used throughout the whole process. The nanosized Y_2O_3:Er^{3+}-Yb^{3+} materials were prepared by using different precipitant agents in a facile hydrothermal method, and schematic of the process is shown in Figure 1. Firstly, a precipitant agent solution (A1) was prepared by dissolving Lithium Hydroxide and Thiourea (LiOH-$SC(NH_2)_2$) and either Lithium Hydroxide and Urea (LiOH-$CO(NH_2)_2$) or only LiOH or only Urea (the last three samples as reference samples) in 200 mL of deionized water in a Teflon container under strong stirring. In another vessel (A2) the rare earth nitrates were dissolved in 50 mL of deionized water by stirring. Then dissolved precursor salts (A2) were added to the precipitant agent solution (A1). Four different samples were obtained of the Y_2O_3 host doped with Er^{3+}:Yb^{3+} in a relation of 1 : 2 mol%. In each case, the mixing was made at room temperature and the pH value was adjusted slowly under vigorous stirring so that the active ions are uniformly dispersed. The resultant solution was transferred into a sealed autoclave and maintained at 100°C during 20 h. After that, the obtained precipitate was washed with water and dried in an oven at 100°C for 24 h. Finally, the resultant powders were annealed in a furnace at 500°C for 1.5 h and 1000°C for 3 h, using a heating rate of 10°/min. After annealing, they were cooled down naturally at room temperature under air atmosphere.

2.2. Structural and Morphological Characterization. The crystalline structure of the nanophosphors was characterized by X-ray diffraction (XRD) using a θ-θ Bruker D-8 Advance diffractometer, having the Bragg-Brentano geometry using CuKα radiation (λ = 1.5405 Å), a Ni 0.5% CuKβ filter in the secondary beam, and a one-dimensional position sensitive silicon strip detector (Bruker, Lynxeye). Diffraction intensity as a function of the angle 2θ was measured between 5° and 80° in steps of 0.02° with a count time of 53 s. Size and morphology of powders have been examined using JEOL JSM-6060LV scanning electron microscope (SEM) operated at 28 kV. The samples were prepared by placing a drop of dilute alcohol dispersion of nanophosphors on the surface of the copper stub. The electron microscope is used in the EDX mode to obtain the composition of the samples. Fourier transform infrared (FT-IR) spectroscopic measurements were obtained using a Bruker FT-IR spectrometer (model: TENSOR 37).

2.3. Absorption and Photoluminescence. The optical spectra were measured with spectrophotometer of Agilent Technologies Model Cary 5000 UV-Vis-NIR. The photoluminescence (PL) characterization was performed using a CW semiconductor laser diode as a pump source centered at 980 nm. The fluorescence emission was analyzed with a monochromator Acton Pro 2300i from Acton Research and a R955 Hamamatsu photomultiplier tube. The system was controlled with a PC where emission spectra were recorded. Fluorescence lifetimes were measured using CW laser diode, the monochromator, and photomultiplier connected to a Teledyne LeCroy Digital Oscilloscope. All measurements were performed at room temperature. Samples were supported in 1 mm capillary tube in order to guarantee the same quantity

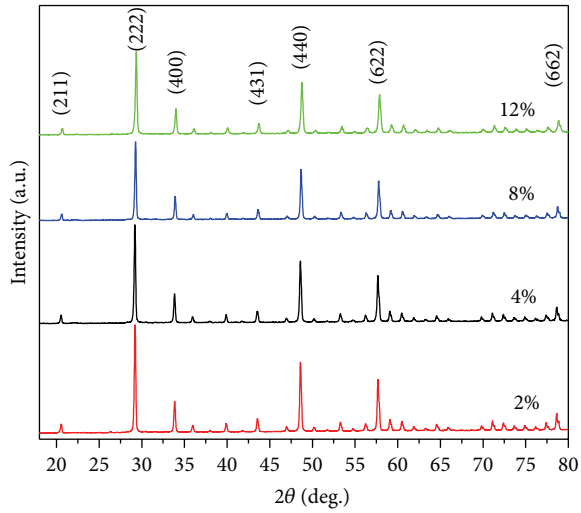

Figure 2: XRD patterns of Y_2O_3:Er^{3+}-Yb^{3+} powders for different precipitant agents.

of excited material. Special care was taken to maintain the alignment of the setup in order to compare the intensities of the upconverted signal between different characterized samples.

3. Results and Discussion

3.1. Structural Characterizations of Nanophosphors. The XRD patterns obtained for all Y_2O_3:Er^{3+}-Yb^{3+} powder samples, synthesized by using different precipitant agents (Thiourea-LiOH/Urea-LiOH/Urea/LiOH), are shown in Figure 2. For all samples the XRD peaks were indexed according to the standard JCPDS #71-0099 corresponding to the cubic structure for Y_2O_3 phase [space group Ia-3(206)]. For all precipitant agents seven main peaks are observed corresponding to the planes (211), (222), (400), (431), (440), (622), and (662). The samples obtained with Urea-LiOH and only LiOH present a segregation of phase (∗) which corresponds to Lithium Hydroxide hydrate (JCPDS #25-0486). All samples present (222) as a main peak and as the preferential orientation, this peak was around $2\theta = 29.2^{\circ}$. Cell parameters estimated form XRD diffraction patterns were 10.526 (Urea), 10.572 (Urea-LiOH), 10.582 (Thiourea-LiOH), and 10.608 Å (LiOH) as shown in Table 1. The average crystallite sizes were obtained by using Scherrer's formula:

$$D = \frac{(0.9)\,\lambda}{\beta \cos(\theta)}. \quad (1)$$

Here, λ is the X-ray wavelength, β is the corrected half-width of the strongest diffraction peak, and θ is the diffraction angle. The crystallite sizes for the four samples prepared with different precipitant agents are presented in Table 1. These measurements indicate that the inclusion of Li^+ ions stimulates the growth of Y_2O_3 nanocrystals.

3.2. Morphological Characterization of the Nanophosphors. SEM micrographs in Figure 3 show the morphology of the

Table 1: Crystallite size, lattice parameters, and cell volume for samples prepared with different precipitant agents.

Precipitant agent	Crystallite size (nm)	Lattice parameters (Å)	Cell volume $(Å)^3$
Thiourea-LiOH	41.5	$a = 10.582$	1184.95
Urea-LiOH	41	$a = 10.572$	1181.60
LiOH	39.5	$a = 10.608$	1193.71
Urea	32.5	$a = 10.526$	1166.25

Y_2O_3:Er^{3+}-Yb^{3+} phosphors obtained with different precipitant agents. The samples prepared with Thiourea-LiOH present relatively uniform particles with regular spherical shape with a narrow size distribution around 300 nm, as can be seen in the histogram. The samples prepared with Urea-LiOH present spherical particles around 435 nm, but for this sample irregular big particles can be seen as well. Phosphors obtained with only LiOH show small particles around 440 nm as well as big particles of more than 1 micron in size. The sample prepared with only Urea presents principally regular spherical particles, but also few bigger particles are present. The diameter sizes of the spherical particles are around 400 nm. The type of precipitant agent does not affect significantly the morphology of the particles, but the size and size distribution could be controlled by precipitant agent variations. The EDX analysis shown in Figure 4 confirms the presence of sulfur in the sample synthesized with Thiourea and Lithium Hydroxide; the measurements for this synthesized sample give an average of 0.65 weight % of sulfur content. FT-IR spectra of the Y_2O_3:Er^{3+}-Yb^{3+} synthesized samples with different precipitant agents are shown in Figure 5. The peaks at 416, 464, and 557 cm^{-1} are attributed to Y-O vibrations in the Y_2O_3 structure [16, 20, 24]. The position of the peaks does not change for samples prepared with or without LiOH, but a slight diminution in the peak intensity can be observed. This reduction in the Y-O vibrational band intensity could be due to the decrease of Y^{3+} sites owing to Li^+ ions inclusion in the Y_2O_3 lattice [24]. The bands around 1450 cm^{-1} correspond to CO groups [20, 24, 25] and their intensity decreases when the sample is prepared with Thiourea+LiOH as precipitant agents. Such CO groups reduction leads to a decrease of PL quenching centers, which in turn lead to an enhancement of the upconversion emission intensity [5, 18, 20, 24–26]. Noteworthy, in all prepared samples no observable bands around 3400 cm^{-1} were found that suggest OH groups are not present or are under the detection limit; see Figure 5. The peak around 1130 cm^{-1} in spectrum of the sample obtained with Thiourea-LiOH corresponds to $(SO_4)^{2-}$ ions [24, 26]. It suggests the presence of sulfur absorbed on the Y_2O_3:Er^{3+}-Yb^{3+} surface.

3.3. Absorption and Photoluminescence Studies

3.3.1. Absorption Spectra. Absorption spectra of Y_2O_3:Er^{3+}, Yb^{3+}, obtained from different precipitant agents, are shown in Figure 6. These spectra are consistent with the typical absorption transitions presented in the same host [5, 10,

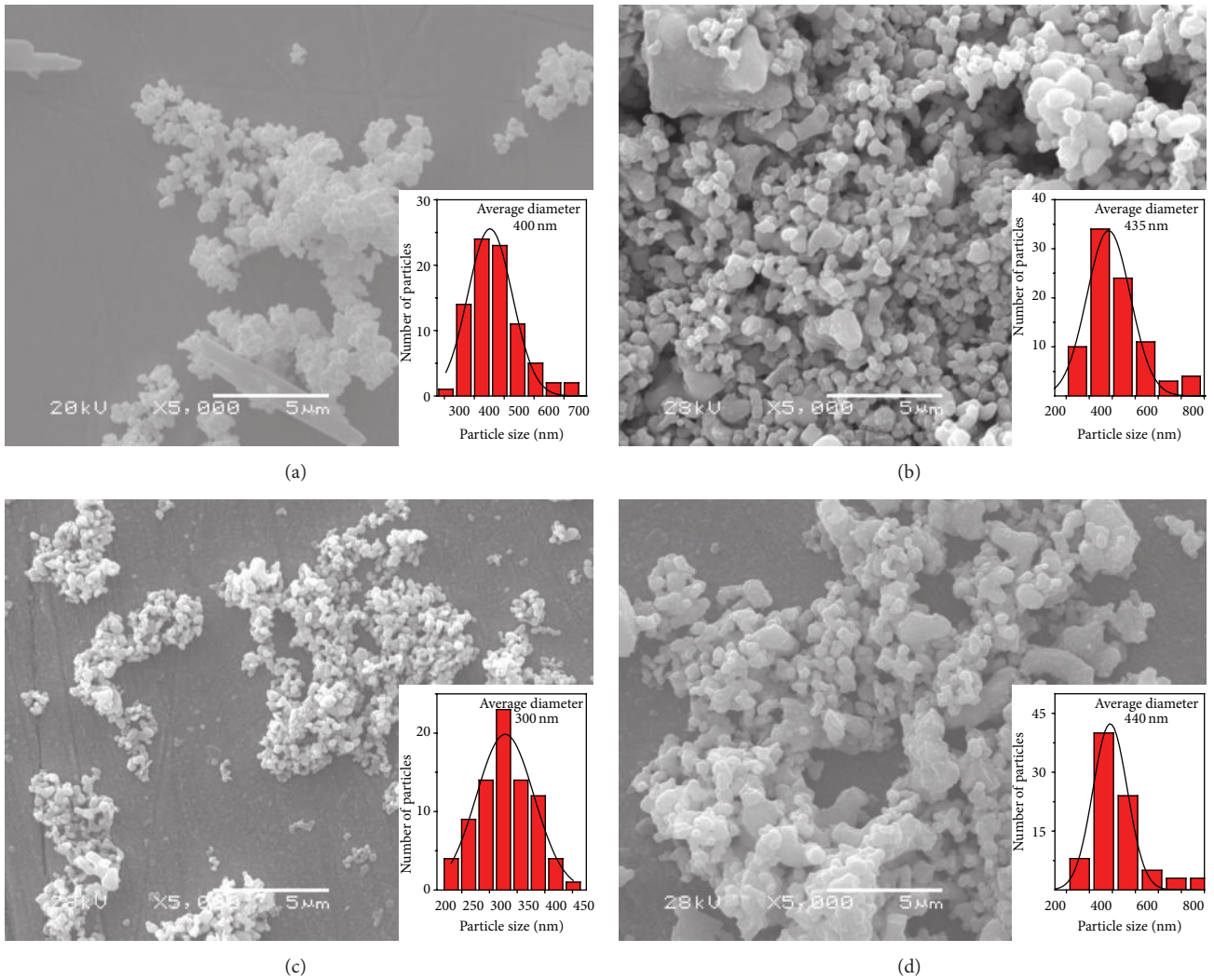

FIGURE 3: SEM images of Y_2O_3:Er^{3+}-Yb^{3+} nanoparticles for different precipitant agents, (a) Urea, (b) Urea-LiOH, (c) Thiourea-LiOH, and (d) LiOH.

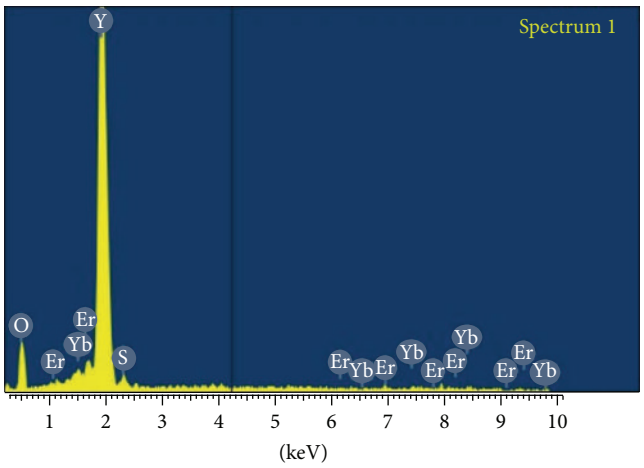

Full scale 476 cts cursor: 4.228 keV (5 cts)

FIGURE 4: EDX analysis for the sample prepared with Thiourea and Lithium Hydroxide.

18, 20, 27] and different hosts [18, 28], including the same doping ions. The main absorption bands are identified and labeled with the corresponding transition coming from the ground states of Er^{3+} ($^4I_{15/2}$) and Yb^{3+} ($^2F_{7/2}$) ions. The main Er^{3+} absorption peaks are 1445 nm ($^4I_{13/2}$); the four folds at 906, 947, 976, and 1028 nm result from the overlap between Er^{3+} ($^4I_{11/2}$) levels with the broad absorption band of Yb^{3+} ($^2F_{5/2}$) ion. The sample obtained with only LiOH exhibits the strongest absorption bands. Other important peaks are at 800 nm ($^4I_{9/2}$), 654 nm ($^4F_{9/2}$), 538 nm ($^4S_{3/2}$), and 522 nm ($^2H_{11/2}$). The changes on the positions of the Er^{3+} NIR absorption peaks around 1450 nm as precipitant agent changes are worth noticing. For Urea the manifolds are at 1463, 1475, 1496, and 1535 nm and the main peak is at 1574 nm, whereas for LiOH or Urea-LiOH the peaks are at 1419, 1475, 1535, and 1574 nm and the main peak is located at 1445 nm. In the case when the sample is prepared with Thiourea+LiOH the former two peaks are suppressed and two new peaks

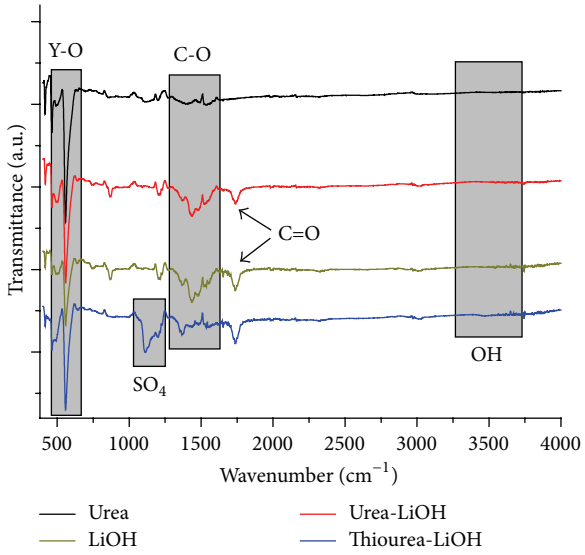

FIGURE 5: FT-IR spectra of Y_2O_3:Er^{3+}-Yb^{3+} phosphors for different precipitant agents.

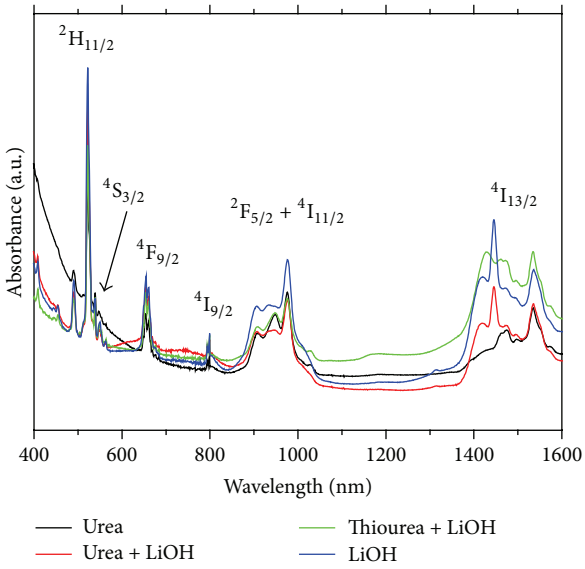

FIGURE 6: Absorbance spectra of Y_2O_3:Er^{3+}-Yb^{3+} nanophosphors for different precipitant agents.

at 1461 and 1428 nm appear as the main peaks in the NIR absorption. This indicates that the local crystal field around the Er^{3+} ions changes as the precipitant agent changes.

3.3.2. Photoluminescence. Emission spectra of the Y_2O_3:Er^{3+}-Yb^{3+} nanophosphors prepared with different precipitant agents are shown in Figure 7. Excitation for the four samples was at 980 nm. All the samples present red and green emissions. The red band centered on 660 nm corresponds to the $^4F_{9/2} \rightarrow {}^4I_{15/2}$ transition. The main green band centered on 563 nm corresponds to the $^4S_{3/2} \rightarrow {}^4I_{15/2}$ transition and the second green band at 522 nm to

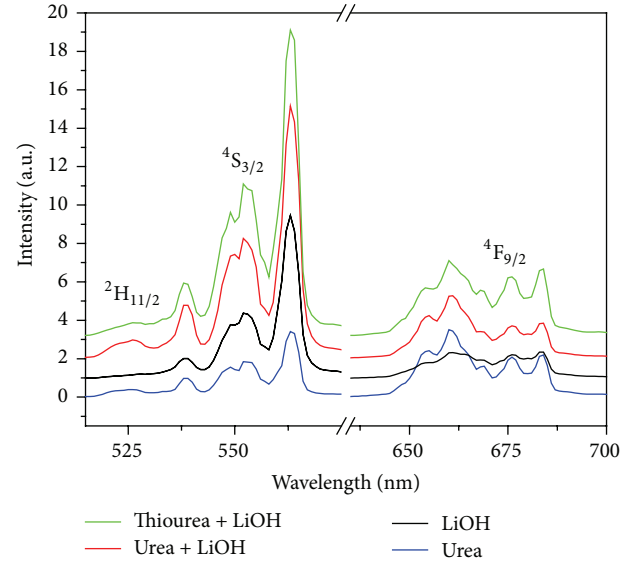

FIGURE 7: Upconversion emission spectra for Y_2O_3:Er^{3+}-Yb^{3+} nanophosphors using different precipitant agents.

the $^2H_{11/2} \rightarrow {}^4I_{15/2}$ transition of Er^{3+} ions. The sample which exhibits the most intense green emission corresponds to the one obtained with Thiourea and Lithium Hydroxide. The sample where the precipitant agent was only Urea presents the lowest emission. When LiOH is used instead of Urea, a small increment on emission intensity is observed. A greater enhancement is reached when the mixture of Urea-LiOH is used as precipitant agent. However, the best results are accomplished by changing Urea to Thiourea in the former case. The increment observed when the sample is obtained with LiOH instead of Urea could be due to the insertion of Li ions into the Y_2O_3 host lattice, in agreement with previous works [18, 20, 23–26, 29, 30]. When Thiourea is utilized in the synthesis process, improvement on luminescence emission due to S ions is expected [22]. The huge enhancement observed when the mixture Thiourea-LiOH is used as precipitant agent could be due to the formation of $(SO_4)^{2-}$ groups on the crystallites' surface [29, 31]. The formation of $(SO_4)^{2-}$ groups reduces quenching CO groups (see Figure 5), and the insertion of Li ions can induce a reduction of charge related defects in the ytterbium/erbium substituted sites into the nanocrystals [18, 24–26, 29, 32], and that in turn will cause the enhancement of upconversion intensity [24–26, 29, 32]. In summary, inclusion of Li and S ions leads to an appreciable enhancement of photoluminescent emission.

The energy levels diagram of Yb^{3+} and Er^{3+} ions is presented in Figure 8. In this figure, the principal upconversion processes required to produce red (660 nm) and green (563 and 522 nm) emissions are depicted. Dependence of the upconversion emission spectra on excitation power is presented for the red and green bands in Figure 9(a). The sample prepared with Thiourea and Lithium Hydroxide was selected because it presented the best emission spectra. An approximation to the number of NIR photons, n, that are necessary to populate the excited emitting state can

Table 2: Decay times of energy levels as a function of different precipitant agents.

Emission transition	Peak wavelength	Thiourea-LiOH	Urea-LiOH	LiOH	Urea
$^4S_{3/2} \rightarrow {}^4I_{15/2}$	563 nm	0.807 ms	0.577 ms	0.574 ms	0.515 ms
$^4F_{9/2} \rightarrow {}^4I_{15/2}$	660 nm	1.170 ms	0.863 ms	0.856 ms	0.611 ms
$^2F_{5/2} \rightarrow {}^2F_{7/2}$	1030 nm	1.780 ms	1.30 ms	1.280 ms	1.090 ms
$^4I_{13/2} \rightarrow {}^4I_{15/2}$	1535 nm	13.50 ms	9.960 ms	8.820 ms	8.110 ms

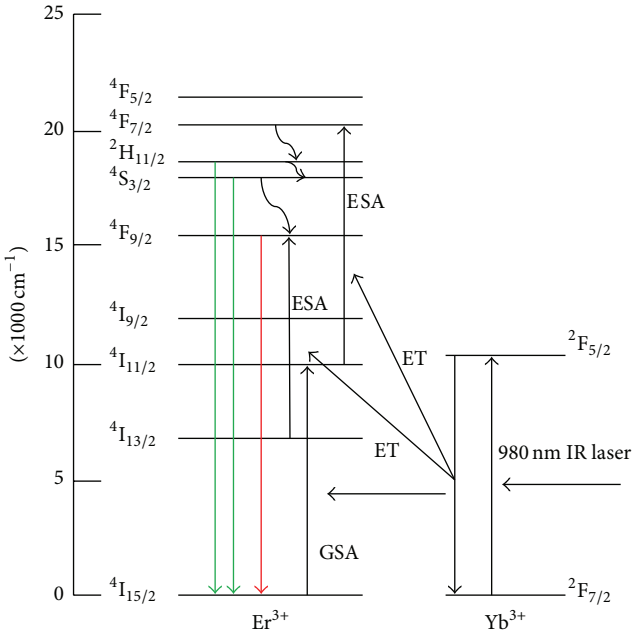

Figure 8: Energy level diagram of Yb^{3+}-Er^{3+} system for upconversion mechanism under 980 nm excitation.

be obtained by the relation $I_{upc} = kI^n_{pump}$, where the upconverted emission intensity (I_{upc}) is proportional to the absorbed pumping power (I_{pump}) in the NIR. The log-log plots in Figure 9(b) depict such relationship. Values of n were obtained by fitting the data to a straight line, where slope corresponds to n, being for green and red emissions, in the case of Thiourea-LiOH, 1.5 and 1.3, respectively. The other values of n for Urea-LiOH, LiOH, and Urea as precipitant agents were 1.4, 1.3, and 1.5 and 1.2, 1.2, and 1.3 for green and red bands, respectively. These n values indicate that more than one photon is required to promote the electron to the $^2H_{11/2} + {}^4S_{3/2}$ and $^4F_{9/2}$ emitting levels. Now, from the levels diagram in Figure 8 an n value of two or at least close to it is expected. The lower values of n suggest that nonradiative processes behind the final visible emission are more complex than a simple Yb to Er direct energy transfer starting at the $^4I_{11/2}$ level. After the initial excitation of Er^{3+} and Yb^{3+} ions, Ground State Absorption (GSA) at the $^4I_{11/2}$ Er^{3+} level as well as energy migration among Yb^{3+} ions can increase the rate at which the $^4I_{11/2}$ Er^{3+} level is repopulated without requiring an excitation photon. Thus for each process it is possible to reach the Er^{3+} $^2H_{11/2} + {}^4S_{3/2}$ and $^4F_{9/2}$ emitting levels by absorbing a single excitation photon. That will lead on the stationary regime to an average requirement of excitation photons lower than $n = 2$. Thus, the obtained values suggest that GSA and energy migration among Yb ions are quite important, and that at the end allows a better performance of the phosphor.

The lifetimes of the energy levels for the Y_2O_3:Er^{3+}-Yb^{3+} nanocrystals for the different precipitant agents, for visible and NIR regions, have been measured and presented in Table 2. The sample synthesized using Thiourea-LiOH as precipitant agent shows the highest lifetimes in visible and IR regions, which explains the results of emission spectra seen in Figure 7, where the best intensity of luminescence in the visible region corresponds to the sample prepared with Thiourea and Lithium Hydroxide. The next sample that has better lifetimes and better emission corresponds to the sample with Urea and Lithium Hydroxide as precipitant agent. The sample that has the lower emission and decay times corresponds to the sample prepared with Urea as precipitant agent. When the sample is obtained with only LiOH instead of Urea the lifetimes increase and when the sample is prepared with Urea-LiOH the lifetimes are better than for the sample prepared only with LiOH, but the highest lifetimes in visible and IR regions correspond to the sample prepared with Thiourea and Lithium Hydroxide. It is worth noticing that this lifetime behavior agrees with the fact that all the levels involved increase. That suggests that in fact Er^{3+} GSA as well as energy migration among Yb^{3+} ions is taking place. An additional channel for lifetime enhancement might be due to the fact that incorporation of both Li and S ions into the lattice and surface of the Y_2O_3 nanocrystallites leads to the reduction of PL quenching OH and CO groups.

The CIE chromaticity diagram for PL of the prepared Y_2O_3:Er^{3+}-Yb^{3+} nanophosphors is presented in Figure 10; for that the excitation was at 980 nm. The CIE chromaticity coordinates of (0.352, 0.643), (0.368, 0.622), (0.373, 0.615), and (0.399, 0.586) correspond to Thiourea-LiOH, Urea-LiOH, only LiOH, and only Urea as precipitant agents, respectively. As observed in Figure 10 the green color luminescence intensity of the phosphors increases by preparing the samples with Thiourea and Lithium Hydroxide. It shifts from yellow-green (Urea) to yellowish-green (Thiourea-LiOH).

4. Conclusions

It has been shown that a correct selection of precipitant agent in the hydrothermal method is important. By using a mixture of Thiourea and Lithium Hydroxide inclusion of both sulfur and lithium ions into the nanocrystals is achieved. SEM results show that the samples do not change their morphology significantly, but the particles sizes for the Thiourea+LiOH

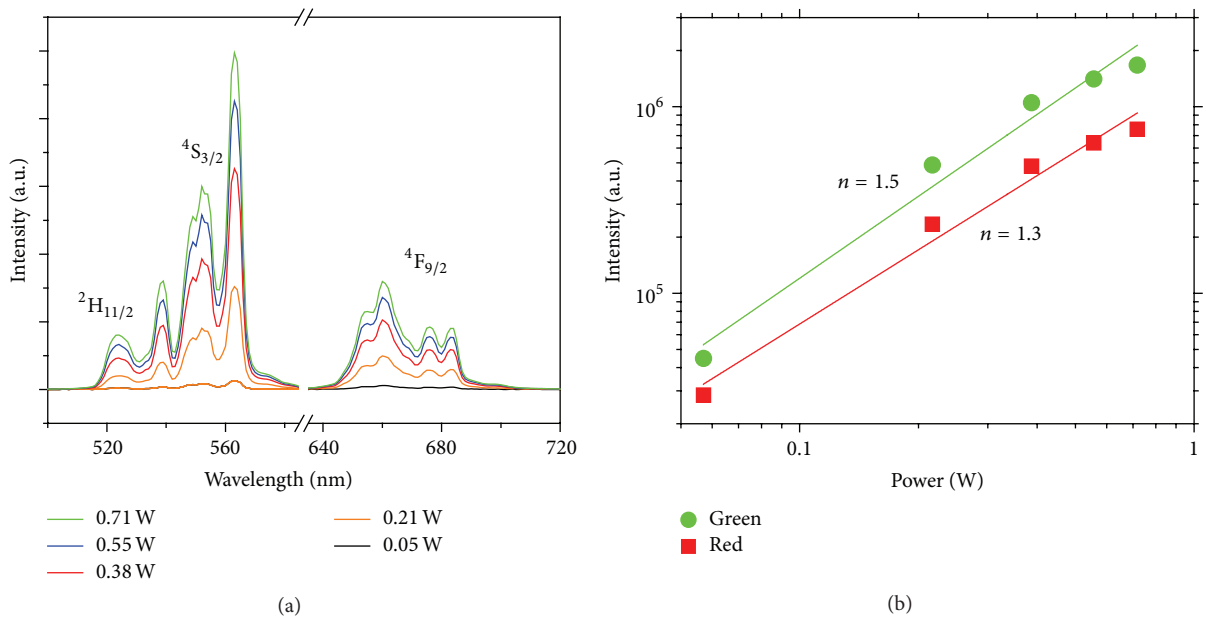

FIGURE 9: (a) Upconversion emission intensity versus excitation pump power at 980 nm, (b) dependence of the green and red upconversion emission for the Thiourea-LiOH sample.

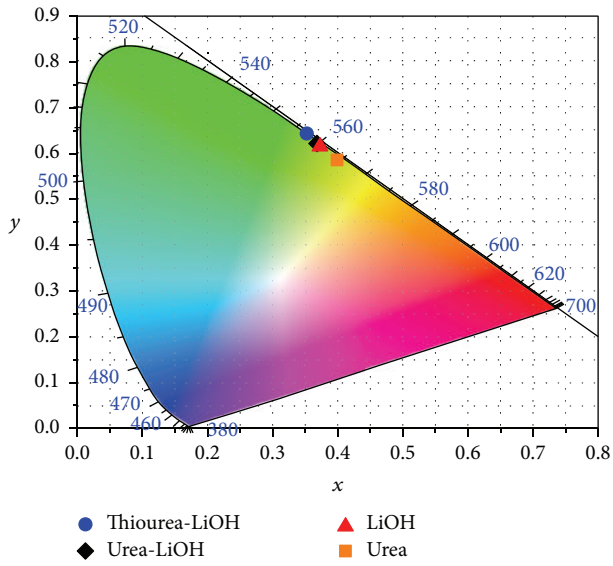

FIGURE 10: CIE chromaticity diagram of Y_2O_3:Er^{3+}-Yb^{3+} for different precipitant agents.

prepared sample are smaller than for the other precipitant agents. Inclusion of sulfur ions as $(SO_4)^{2-}$ groups on the crystallites surface reduces the CO and OH groups and that in turn reduces the quenching effects on luminescence due to these groups. It was observed that the incorporation of Li improves the visible and NIR Er^{3+} and Yb^{3+} luminescence emissions, probably by enhancing the Er^{3+} GSA and the energy migration among Yb^{3+} ions. This effect has been associated with the distortion of the crystal field around rare earth ions as well as with the creation of localized state in the yttrium oxide matrix, which stimulate the Yb^{3+} to Er^{3+} nonradiative transfer processes. Thus, the use of the Thiourea and Lithium Hydroxide mixture allows the inclusion of Li and S ions into nanocrystals, and this in turn leads to a huge enhancement of upconversion photoluminescence emission.

Conflict of Interests

The authors declare that there is no conflict of interests regarding the publication of this paper.

Acknowledgment

Eder Resendiz-L thanks CONACyT for its support through Scholarship Grant 232056 for Ph.D. studies at Centro de Física Aplicada y Tecnología Avanzada of UNAM.

References

[1] L. F. Johnson and H. J. Gugenheim, "Infrared-pumped visible laser," *Applied Physics Letters*, vol. 19, no. 2, article 44, 1971.

[2] A. Valanne, P. Malmi, H. Appelblom, P. Niemelä, and T. Soukka, "A dual-step fluorescence resonance energy transfer-based quenching assay for screening of caspase-3 inhibitors," *Analytical Biochemistry*, vol. 375, no. 1, pp. 71–81, 2008.

[3] E. Heumann, S. Bar, K. Rademaker et al., "Semiconductor-laser-pumped high-power upconversion laser," *Applied Physics Letters*, vol. 88, no. 6, pp. 1–3, 2006.

[4] A. S. S. de Camargo, J. F. Possatto, L. A. D. O. Nunes et al., "Infrared to visible frequency upconversion temperature sensor based on Er^{3+}-doped PLZT transparent ceramics," *Solid State Communications*, vol. 137, no. 1-2, pp. 1–5, 2006.

[5] A. K. Singh, P. K. Shahi, S. B. Rai, and B. Ullrich, "Host matrix impact on Er^{3+} upconversion emission and its temperature

dependence," *RSC Advances*, vol. 5, no. 21, pp. 16067–16073, 2015.

[6] F. van de Rijke, H. Zijlmans, S. Li et al., "Up-converting phosphor reporters for nucleic acid microarrays," *Nature Biotechnology*, vol. 19, no. 3, pp. 273–276, 2001.

[7] F. Auzel, "Upconversion and anti-stokes processes with f and d ions in solids," *Chemical Reviews*, vol. 104, no. 1, pp. 139–173, 2004.

[8] C. G. Dou, Q. H. Yang, X. M. Hu, and J. Xu, "Cooperative up-conversion luminescence of ytterbium doped yttrium lanthanum oxide transparent ceramic," *Optics Communications*, vol. 281, no. 4, pp. 692–695, 2008.

[9] Y. Qiao and H. Guo, "Upconversion properties of Y_2O_3:Er films prepared by sol-gel method," *Journal of Rare Earths*, vol. 27, no. 3, pp. 406–410, 2009.

[10] A. Martínez, J. Morales, L. A. Díaz-Torres et al., "Green and red upconverted emission of hydrothermal synthesized Y_2O_3: Er^{3+}-Yb^{3+} nanophosphors using different solvent ratio conditions," *Materials Science and Engineering B: Solid-State Materials for Advanced Technology*, vol. 174, no. 1–3, pp. 164–168, 2010.

[11] V. Lojpur, S. P. Ahrenkiel, and M. D. Dramićanin, "Yb^{3+}, Er^{3+} doped Y_2O_3 nanoparticles of different shapes prepared by self-propagating room temperature reaction method," *Ceramics International*, vol. 40, no. 10, pp. 16033–16039, 2014.

[12] R. Dey, V. K. Rai, and A. Pandey, "Green upconversion emission in Nd^{3+}-Yb^{3+}-Zn^{2+}:Y_2O_3 phosphor," *Spectrochimica Acta A*, vol. 99, pp. 288–291, 2012.

[13] Y. Yu, D. Qi, and H. Zhao, "Enhanced green upconversion luminescence in Ho^{3+} and Yb^{3+} codoped Y_2O_3 ceramics with Gd^{3+} ions," *Journal of Luminescence*, vol. 143, pp. 388–392, 2013.

[14] W. Xiantao, Z. Jiangbo, Z. Weiping, L. Yong, and Y. Min, "Cooperative energy transfer in Eu^{3+}, Yb^{3+} codoped Y_2O_3 phosphor," *Journal of Rare Earths*, vol. 28, no. 2, pp. 166–170, 2010.

[15] L. Mancic, V. Lojpur, B. A. Marinkovic, M. H. de Pinho Mauricio, M. D. Dramicanin, and O. Milosevic, "Effect of processing parameters on structural, morphological and optical Y_2O_3:Yb^{3+}/Ho^{3+} powders characteristics," *Advanced Powder Technology*, vol. 25, no. 5, pp. 1449–1454, 2014.

[16] A. Pandey and V. K. Rai, "Pr^{3+}–Yb^{3+} codoped Y_2O_3 phosphor for display devices," *Materials Research Bulletin*, vol. 57, pp. 156–161, 2014.

[17] R. S. Yadav, R. K. Verma, A. Bahadur, and S. B. Rai, "Structural characterizations and intense green upconversion emission in Yb^{3+}, Pr^{3+} co-doped Y_2O_3 nano-phosphor," *Spectrochimica Acta Part A: Molecular and Biomolecular Spectroscopy*, vol. 137, pp. 357–362, 2015.

[18] A. K. Singh, S. K. Singh, and S. B. Rai, "Role of Li^+ ion in the luminescence enhancement of lanthanide ions: favorable modifications in host matrices," *RSC Advances*, vol. 4, no. 51, pp. 27039–27061, 2014.

[19] R. Yadav, S. K. Singh, R. K. Verma, and S. B. Rai, "Observation of multi-mode: upconversion, downshifting and quantum-cutting emission in Tm^{3+}/Yb^{3+} co-doped Y_2O_3 phosphor," *Chemical Physics Letters*, vol. 599, pp. 122–126, 2014.

[20] B. Y. Kokuoz, K. Serivalsatit, B. Kokuoz, O. Geiculescu, E. McCormick, and J. Ballato, "Er-doped Y_2O_3 nanoparticles: a comparison of different synthesis methods," *Journal of the American Ceramic Society*, vol. 92, no. 10, Article ID 22472253, pp. 2247–2253, 2009.

[21] G. Wang, W. Qin, J. Zhang et al., "Enhancement of violet and ultraviolet upconversion emissions in Yb^{3+}/Er^{3+}-codoped YF3 nanocrystals," *Optical Materials*, vol. 31, no. 2, pp. 296–299, 2008.

[22] A. G. Ali, B. F. Dejene, and H. C. Swart, "Synthesis and characterization of Y_2O_3:Eu^{3+} phosphors using the Sol-Combustion method," *Physica B: Condensed Matter*, vol. 439, pp. 181–184, 2014.

[23] H. Liang, G. Chen, H. Liu, and Z. Zhang, "Ultraviolet upconversion luminescence enhancement in Yb^{3+}/Er^{3+}-codoped Y_2O_3 nanocrystals induced by tridoping with Li^+ ions," *Journal of Luminescence*, vol. 129, no. 3, pp. 197–202, 2009.

[24] K. Mishra, S. K. Singh, A. K. Singh, and S. B. Rai, "Frequency upconversion in Er^{3+} doped Y_2O_3 nanophosphor:Yb^{3+} sensitization and tailoring effect of Li^+ ion," *Materials Research Bulletin*, vol. 48, no. 10, pp. 4307–4313, 2013.

[25] A. Pandey, V. K. Rai, and K. Kumar, "Influence of Li^+ codoping on visible emission of Y_2O_3:Tb^{3+}, Yb^{3+} phosphor," *Spectrochimica Acta—Part A: Molecular and Biomolecular Spectroscopy*, vol. 118, pp. 619–623, 2014.

[26] D. Li, Y. Wang, X. Zhang et al., "Effect of Li^+ ions on enhancement of near-infrared upconversion emission in Y_2O_3:Tm^{3+}/Yb^{3+} nanocrystals," *Journal of Applied Physics*, vol. 112, Article ID 094701, 2012.

[27] A. Martínez, J. Morales, P. Salas, C. Angeles-Chávez, L. A. Díaz-Torres, and E. De la Rosa, "Synthesis and photoluminescence of Y_2O_3:Yb^{3+}–Er^{3+} nanofibers," *Microelectronics Journal*, vol. 39, no. 3-4, pp. 551–555, 2008.

[28] P. Salas, C. Angeles-Chávez, J. A. Montoya et al., "Synthesis, characterization and luminescence properties of ZrO_2:Yb^{3+}-Er^{3+} nanophosphor," *Optical Materials*, vol. 27, no. 7, pp. 1295–1300, 2005.

[29] T. López-Luke, E. De La Rosa, I. Campos Villalobos et al., "Improving pure red upconversion emission of Co-doped Y_2O_3:Yb^{3+}-Er^{3+} nanocrystals with a combination of sodium sulfide and surfactant Pluronic-F127," *Journal of Luminescence*, vol. 145, pp. 292–298, 2014.

[30] Y. Bai, Y. Wang, G. Peng et al., "Enhanced white light emission in Er/Tm/Yb/Li codoped Y_2O_3 nanocrystals," *Optics Communications*, vol. 282, no. 9, pp. 1922–1924, 2009.

[31] J. He, X. Lia, S. Liu, Q. Zhu, J.-G. Li, and X. Sun, "Effects of pre-treatment of starting powder with sulfuric acid on the fabrication of yttria transparent ceramics," *Journal of the European Ceramic Society*, vol. 35, no. 8, pp. 2369–2377, 2015.

[32] H. Liang, Y. Zheng, Z. Chen et al., "Enhancement of upconversion luminescence of Y_2O_3:Er^{3+} nanocrystals by codoping Li^+–Zn^{2+}," *Journal of Alloys and Compounds*, vol. 509, no. 2, pp. 409–413, 2011.